DOI: 10.61782/fa.2023.0731

forum acusticum 2023

ANALYSIS OF IMPEDANCE EFFECTS ON HEAD-RELATED TRANSFER FUNCTIONS OF 3D PRINTED PINNA AND EAR CANAL REPLICAS

Fabio Di Giusto[1,2*] **Daniel Sinev**[3,4] **Katharina Pollack**[5]
Sjoerd van Ophem[1,2] **Elke Deckers**[6,2]
[1] KU Leuven, Department of Mechanical Engineering, Heverlee, Belgium
[2] Flanders Make@KU Leuven
[3] Sonova Consumer Hearing GmbH, Wedemark, Germany
[4] Institut für Kommunikationstechnik, Leibniz Universität Hannover, Hannover, Germany
[5] Acoustics Research Institute, Austrian Academy of Sciences, Vienna, Austria
[6] KU Leuven, Campus Diepenbeek, Department of Mechanical Engineering, Diepenbeek, Belgium

ABSTRACT

Numerical simulations of Head-Related Transfer Functions (HRTFs) are an efficient method to obtain the binaural filters necessary for spatial audio reproduction. State-of-the-art simulated HRTFs are generally computed at the blocked ear canal of scanned geometries using rigid acoustic boundary conditions. This choice is justified by measurements of human skin impedance up to 6 kHz, showing an acoustically rigid behaviour. The limited bandwidth of these measurements is due to the difficulty in reliably measuring skin impedance up to the highest audible frequency. Furthermore, rigid boundary conditions can lead to discrepancies between measured and simulated HRTFs at high frequencies. To assess the effect of the outer ear acoustic impedance characteristics on the HRTFs, 3D printed replicas of individual pinna and ear canal geometries are used in this study, allowing the creation of samples which can be characterised in an impedance tube up to high frequencies. Their measured impedance is used as a boundary condition in simulations, which outcomes relate to a lower spectral distortion to measured transfer functions in comparison to rigid computations. The perceptual effect of modelling impedance in the simulations is however found to be minimal.

*__Corresponding author__: *fabio.digiusto@kuleuven.be.*

Keywords: *HRTFs, spatial audio, ear canal, acoustic impedance.*

1. INTRODUCTION

Immersive audiovisual technologies, such as Virtual Reality (VR), require accurate rendering of acoustic scenes, commonly obtained through headphone playback of audio filtered with Head-Related Transfer Functions (HRTFs). Correct individual auditory cues in these binaural filters are necessary for the most realistic rendering [1]. Although generally measured, HRTFs can be simulated on scanned geometries using various approaches, e.g. the Finite Element Method (FEM) or Boundary Element Method (BEM). The HRTFs are typically computed at the entrance of the blocked ear canal using acoustically rigid Boundary Conditions (BCs) [2]. This choice is motivated by impedance tube measurements of human skin and of a dummy head material between 1 kHz and 6 kHz, showing an acoustically rigid behaviour [3, 4]. Applying the latter results as impedance BCs in BEM computations is reported not to increase the match to measured HRTFs compared to rigid simulations [4]. Thus, it is concluded that the HRTFs are mainly affected by the ear shape, while the impedance tends to modify the amplitude of their spectral features. However, the limited frequency range of these studies, due to difficulties in the measurements, raises questions about the validity of using rigid BCs in HRTFs simulations on the full audible range. A recent study used an optimisation approach to find optimal impedance

values that produce a better match of numerical HRTFs to measured data up to 16 kHz [5]. However, a single impedance value is estimated on the geometry, and discrepancies between experimental and numerical HRTFs unrelated to impedance mismatch might also be compensated, leading to potentially unrealistic impedance values.

Recent advances in impedance tubes made it possible to extend their operating range up to 20 kHz by using MEMS microphones and a small inner tube diameter [6]. Therefore, the effect of impedance BCs on simulated HRTFs can be tested up to high frequencies. This paper aims at assessing the effect of acoustic material properties on simulated HRTFs by comparing numerical results with rigid and impedance BCs to measured data. The 3D printed outer ear replicas of a subject up to the eardrum are studied, deriving from a database of human geometries [7], to avoid reliability issues related to direct measurements on human subjects [8]. Since the focus is on the spectral features of the HRTFs, which are mainly generated by the pinnae [9], Pinna-Related Transfer Functions (PRTFs) rather than full HRTFs are analysed, given the lower complexity of computations relating to the outer ear alone. Objective metrics are used to assess the difference between measured and simulated data, and determine if including impedance BCs improves the numerical results. Furthermore, a perceptually inspired metric is used to assess whether PRTFs computed with rigid and impedance BCs lead to a similar spatial sound perception.

This paper is part of a three-paper study in which measured and simulated data on the same outer ear replicas and other individual geometries are analysed [10, 11].

2. METHODS

2.1 Manufacturing of Outer Ear Replicas

Using the scanned geometry of the 9^{th} subject from the IHA database [7], outer ear replicas compatible with the GRAS KEMAR artificial head were created in two pieces [8], i.e. pinnae and ear canals. The pinnae were 3D printed in two materials, i.e. a rigid white resin and a flexible black resin, to assess the effect of their acoustic impedance. The ear canals were cast in silicone using 3D printed negative ear canal shapes, including a microphone mounted in a custom holder at the eardrum position. Additional details on the manufacturing process can be found in [8, 11]. Cylindrical samples of the employed materials, with a diameter of 8 mm and lengths of 5 mm, 10 mm and 25 mm, were created to measure their acoustic properties.

2.2 Measurements and Simulations

2.2.1 *Sample Impedance*

The specific acoustic impedance (Z_s) of the material samples was measured between 20 Hz and 20 kHz using an impedance tube with inner diameter of 8 mm based on 16 MEMS microphones [6]. Prior to the measurement the Z calibration procedure was conducted [12], based on calculating a propagation matrix from three reference measurements of resonance-free loads and using them to solve an overdetermined system and obtain Z_s at the termination. The Z_s and reflection factor ($R = \frac{Z_s - Z_0}{Z_s + Z_0}$) of the calibration cases are shown in Tab. 1, in which $Z_0 = \rho c$ is the characteristic impedance of air, ρ the density of air and c the speed of sound. $Z_{s,\text{o}}$ and R_o are derived from the analytical solution of a piston in an infinite baffle [6, 13].

Table 1: Z_s and R of the resonance-free loads used for impedance tube calibration [6].

Case	Termination	Z_s	R
rigid	aluminium cap	∞	1
anechoic	long PVC tube	Z_0	0
open-end	open tube	$Z_{s,\text{o}}$	R_o

2.2.2 *Closed Ear Canal*

Acoustic input impedance (Z_in) and pressure transfer function (P_tf) were measured on the left ear canal replica, closing it with a custom ear mould including a source and a receiver. Additional information regarding the measurement procedure can be found in [8].

Matching FEM simulations were performed in COMSOL® on the ear canal geometry closed with a plane at the ear mould location and defining sources and receivers matching the experimental case. Additional information regarding the simulation setup can be found in [8]. Losses due to thermal and viscous dissipation were included using a thermoviscous Boundary Layer Impedance (BLI) condition at the ear canal walls [14], while the remaining BCs were defined as rigid. Furthermore, simulations were carried out applying the measured silicone sample impedance as a BC. The results were computed in linear frequency steps of 0.1 kHz between 0.1 kHz and 20 kHz. The maximum element size (l_max) was defined as $l_\text{max} = \lambda/6$, where λ is the wavelength at the maximum

analysed frequency. The temperature was set to 20 °C, close to its average value during the measurements.

The simulation setup was tested by assessing a similar but simpler case for which an analytical solution is available, i.e. the Z_{in} of a cylinder of radius a rigidly terminated at a length l, with and without considering thermoviscous losses [15]. The values of a and l were defined as 4 mm and 35 mm, respectively, similar to the ear canal replica dimensions. A FEM simulation matching this simplified case was defined, using the same parameters as the ear canal simulation, including losses with the BLI condition. For the latter case and the lossy analytical solution, the formulation is based on the assumption of wide tubes, i.e. $a \gg \max\left(a_v = (l_v\lambda)^{0.5}, a_h = (l_h\lambda)^{0.5}\right)$, where l_v and l_h are the characteristic lengths of viscous and thermal effects, respectively [15]. This is considered to be satisfied since $a_v < a_h \approx 0.37$ mm at 100 Hz, while $a = 4$ mm.

2.2.3 *Pinna-Related Transfer Functions*

Measurements on the outer ear replicas mounted on a GRAS cheek simulator, which has an approximately circular geometry with a radius of 60 mm, were conducted in an anechoic room. The cheek simulator was clamped to a turntable with the ear facing a loudspeaker mounted in a wall, its centre was at the same height and at a distance of 1.66 m from the loudspeaker centre. The turntable was rotated on the horizontal plane in steps of 5° between −90° and 90° from the position directly facing the loudspeaker. The frontal plane was measured by rotating the ear by 90° along an axis passing through the ear canal centre and repeating the acquisition. To be in line with common HRTFs conventions, the measurement positions were converted to the interaural-polar coordinate system [2], defined by the azimuth angle $(\theta) \in (-180°, 180°]$, the elevation angle $(\phi) \in [-90°, 90°]$ and the distance (r), with $(\theta, \phi) = (0°, 0°)$ indicating a position frontal to the head and positive θ and ϕ relating to left and above horizontal plane locations, respectively. Measurements were taken with the sensor at the eardrum position and with binaural microphones placed at the ear canal entrance. The manual positioning of the latter could influence the outcome; therefore, the acquisition was repeated two times after repositioning these sensors. Additional information on the measurement procedure, including the normalisation of the data to obtain PRTFs, can be found in [11].

FEM simulations were defined in COMSOL® using the outer ear shape inserted in a circular disc of 60 mm radius, surrounded by an 80 mm radius sphere on which a Perfectly Matched Layer (PML) was used to impose free field conditions [14]. The source was reciprocally defined at the microphone position and the results were evaluated solving the full Helmholtz-Kirchhoff integral equation based on the values computed on the inner side of the PML [14]. The eardrum sensor was modelled by applying a normal velocity to elements at a matching location, while two cases were defined for the binaural microphones. In the first the ear canal entrance was closed with a plane and a normal velocity was applied at the approximate sensor position; in the second a monopole source was placed in the open ear canal at a matching location. The results were computed on a full spherical grid with $r = 1.66$ m and 5° resolution in θ and ϕ, for frequencies between 0.1 kHz and 20 kHz in steps of 0.1 kHz. The $l_{\max}$ was set to 1 mm at the outer ear geometry, to preserve its shape, and $\lambda/6$ in the remaining parts of the domain. The BCs were defined as either fully rigid, or as the measured impedance of the ear canal replica materials. The temperature was set to the value recorded in the room prior to each measurement, i.e. around 18 °C. PRTFs were obtained by normalising the computed results by the pressure of a monopole in free field with a distance of 1.66 m and volume velocity equal to that of the simulated source.

A simplified case with analytical solution to validate this simulation is that of a piston of radius a mounted on a finite circular baffle of radius b and radiating in free field [13]. The values of a and b were chosen to be 4 mm and 60 mm, respectively. These results were used to assess a matching FEM computation of a rigid circular baffle with a piston at its centre. The simulation parameters were defined similarly to the PRTFs case. Given the axial symmetry of this scenario, only horizontal plane positions for $\theta \in [0°, 90°]$ at $r = 1.66$ m were computed.

2.3 Assessment Metrics

2.3.1 *Objective Metrics*

The Spectral Distortion (SD) and the Mean SD (MSD) were used to assess the results. These are defined as:

$$\text{SD}_{i,j} = 20\log_{10}\left(\frac{|H_i|}{|H_j|}\right), \tag{1}$$

$$\text{MSD}_{i,j} = \frac{1}{N_\Psi}\sum_{\Psi}\sqrt{\frac{1}{N_f}\sum_{f}\left(\text{SD}_{i,j}\right)^2}, \tag{2}$$

with H_i and H_j being the compared frequency responses, N_f the number of frequency bins f, and N_Ψ the number of incidence angles $\Psi = (\theta, \phi)$ [2].

2.3.2 *Perceptual Metrics*

Perceptual factors of the PRTFs were evaluated using a sagittal plane localisation model in which template and target Directional Transfer Functions (DTFs), obtained by removing the common directional component from the PRTFs, were used in a virtual localisation experiment [16]. The virtual subject, represented by the template DTFs, localised sound filtered with the target DTFs, and the localisation performance was evaluated in terms of Quadrant Error (QE [%]) and Polar Error (PE [°]), relating to rate of confusion and local precision of the subject's response, respectively. Default values were chosen for the model parameters, while the sensitivity parameter was set to 0.5. The outcome of this model is shown to transfer well to sound perception in VR scenes [1]. Furthermore, ranges of QE and PE of 10 % - 30 % and 33° - 42°, and minimum distance of 3 % and 3° have been used to identify minimal deviant nonindividual HRTFs in relation to an individual one. Spatial sound perception with these HRTFs is shown to relate to low but significant differences in comparison to individual data [1].

3. RESULTS

3.1 Sample Impedance

The measured reflection factors of the impedance tube terminations used for calibration are compared to their analytical values in Fig. 1. Agreement is seen in the amplitude ($|R|$) up to 18 kHz, while noise is observed above this frequency for the measured anechoic and open-end cases. Although the phase of rigid and open-end cases agrees with theory, the measured anechoic termination shows a phase component diverging from its analytical value of 0 rad. This is attributed to limitations of the employed Z calibration procedure for the impedance tube, resulting in an undetermined phase [12]. Given the noise observed at high frequencies, an upper frequency limit of 18 kHz is used in the following analyses.

The measured $|R|$ of all the material samples has values above 0.8 up to 18 kHz, with shorter lengths of the samples relating to higher $|R|$, and a phase component close to 0 rad. These results are in line with skin impedance measurements showing average $|R|$ of 0.97 between 1 kHz and 6 kHz [3]. Mean $|R|$ values in the same frequency range for the 5 mm silicone, white and black material samples are between 0.97 and 0.98; lower values from 0.90 to 0.96 are seen for higher sample lengths. The measured $|Z_s|$ for the material of another dummy head

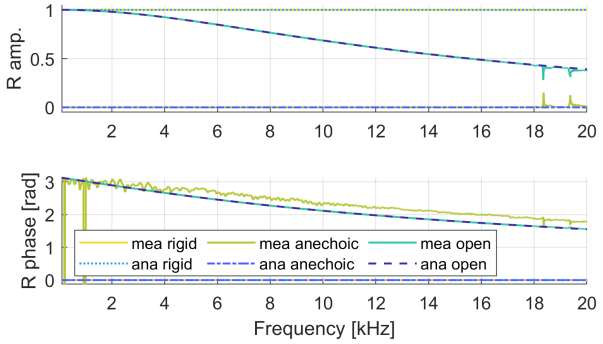

Figure 1: Measured (mea) and analytical (ana) R of the rigid, anechoic and open-end terminations.

tends to 2000 Pa s m^{-1} towards 6 kHz, while oscillating at higher values for lower frequencies [4]. Similar trends but higher $|Z_s|$ tending to 4000 Pa s m^{-1} around 6 kHz are found for the tested samples in different materials.

The repeatability of the acquisition process is assessed by repeating three times the measurement of one sample (10 mm black resin), with and without repositioning it. The results are presented in Fig. 2, where also the measured $|R|$ of the same sample taken on a different day along all the other samples is presented. The repeated measurements without repositioning show stable results up to high frequencies, with maximum deviation in $|R|$ reaching values of 0.03 above 17 kHz, while repositioning the sample relates to higher deviations up to 0.07 at lower frequencies. The single measurement taken along all the other samples shows comparable values, but oscillations around the average $|R|$ of the repeated measurements.

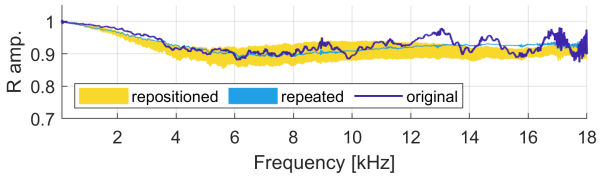

Figure 2: Measured $|R|$ of the 10 mm black resin sample (original) compared to repeated measurements with and without repositioning the sample. The repeated and repositioned results are plotted as areas representing their min and max values.

The 5 mm material samples are further analysed, given that their thickness is close to that of the outer ear replica. Their measured $|R|$ values, presented in Fig. 3,

are similar to each other; the silicone shows the most rigid behaviour, while white and black materials have lower impedance. Oscillations around an average value seem to appear in all measurements. The reason for this behaviour, not noticed in the repeatability test measurements, is not readily apparent and likely due to inaccuracies in the acquisition process, given the high sample impedance requiring ideal measurement conditions for a reliable outcome [12]. All the materials show $|R| \approx 1$ below 2 kHz, and decreasing to lower values towards higher frequencies, although remaining above 0.9. To cope with the oscillating behaviour of the measured data, linear fitting is applied in the frequency range from 0.1 kHz to 18 kHz. The fitted $|R|$ values are also displayed in the plot.

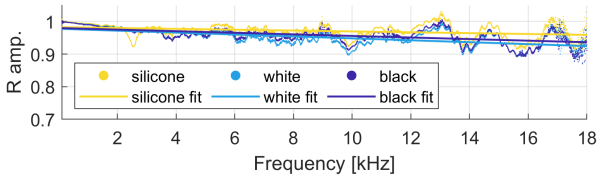

Figure 3: Measured $|R|$ of the 5 mm silicone, white and black resin samples, and linear fit of the data.

3.2 Closed Ear Canals

The analytical and simulated Z_{in} of the rigidly terminated cylinder present small deviations, with MSD below 0.1 dB and maximum level differences of 0.5 dB for the rigid and lossy cases, validating the simulation setup.

The measured Z_{in} of the closed left ear canal replica is compared to results of matching simulations with different BCs in Fig. 4. The value used for the impedance BC at the ear canal walls comes from the measured or linearly fitted 5 mm silicone sample $|R|$. Given the uncertainty in the measured R phase and the rigidity of the materials, a purely resistive impedance is defined as an approximation in this and the following simulations [14]. Measured and simulated results show similar patterns, but discrepancies are noticeable, probably originating from mismatch in simulation parameters from the real scenario. The simulated results with the linearly fitted $|R|$ tend to show the best match to the measured data.

The MSD between the measured Z_{in} and P_{tf} of the closed left ear canal replica and the simulated results with different BCs is summarised in Tab. 2. The cases including impedance BCs show a lower distance from measurement results; the best outcome is obtained using the linearly fitted $|R|$. Higher order polynomial fitting of $|R|$ up to 5$^{\text{th}}$ order shows similar or worse MSD, while using the $|R|$ of the 10 mm and 25 mm samples the MSD increases by at least 1 dB. An attempt has been made to include the R phase component in the impedance BCs, but a sharp increase in MSD by at least 5 dB for all cases is seen.

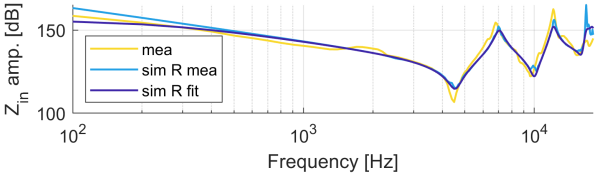

Figure 4: Measured (mea) and simulated (sim) Z_{in} of the closed left ear canal. In the simulations impedance BCs are used from the measured (R mea) or linearly fitted (R fit) silicone sample $|R|$.

Table 2: MSD of the measured and simulated Z_{in} and P_{tf} of the closed left ear canal. In the simulation different BCs are used: rigid (rgd), thermoviscous BLI (tvl), impedance from the measured (R mea) or linearly fitted (R fit) silicone sample $|R|$.

MSD [dB]	rgd	tvl	R mea	R fit
Z_{in}	7.75	6.38	4.47	4.09
P_{tf}	4.81	3.82	2.75	2.41

3.3 Pinna-Related Transfer Functions

The comparison of the simulated and analytical pressure of a piston in a finite circular baffle shows small MSD of 0.3 dB, and maximum level difference of 1.8 dB appearing above 17 kHz, validating the simulation setup.

The measured frontal plane eardrum PRTFs of the left ear in white material are presented in Fig. 5, along with the SD between these and the simulated PRTFs with rigid and impedance BCs deriving from the fitted $|R|$ values. A resonance around 2.6 kHz is observed in the measured data, due to the effect of the ear canal. Large SD is seen at high frequencies between the rigid simulation and the measured data, while the PRTFs computed with impedance BCs show a lower divergence. This is attributed to the lack of damping in rigid simulations. Other

discrepancies could be due to several factors, e.g. measurement error, imperfect geometrical modelling, or differences in the real and virtual microphone locations.

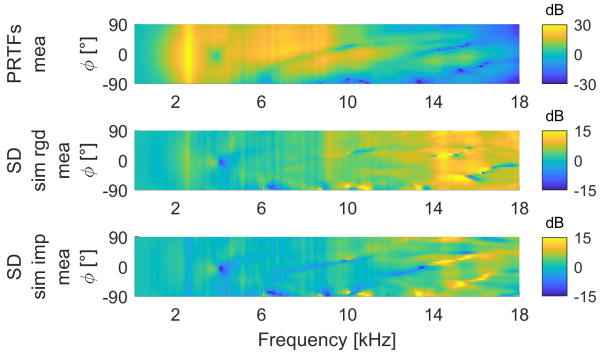

Figure 5: Measured (mea) frontal plane eardrum PRTFs of the left ear and SD between mea and simulated (sim) PRTFs. In the simulations rigid (rgd) and impedance (imp) BCs are used from the linearly fitted silicone and white resin samples $|R|$.

Measured PRTFs acquired with the binaural microphones, and the SD between these and the results of matching simulations, are presented in Fig. 6. The simulations have impedance BCs deriving from the fitted $5\,\mathrm{mm}$ material samples $|R|$, the two source modelling cases are assessed. A better match is seen for measured and simulated data with a monopole source, especially below $10\,\mathrm{kHz}$, while high SD is seen for the modelled closed ear canal case at $4\,\mathrm{kHz}$ and $9\,\mathrm{kHz}$, where two notches in the measured data appear. These are attributed to ear canal reflections due to the binaural microphones, surrounded by foam which only partially occludes the ear canal. This effect is not modelled in the closed ear canal simulations.

The MSD between measured and simulated PRTFs with rigid and impedance BCs are presented in Tab. 3, averaging the results over left and right ear in white and black material. Three cases are presented, relating to the eardrum data, and the two simulations with different source models trying to match the measurements taken with the binaural sensors. Impedance BCs simulations show a mean decrease in MSD of $1.79\,\mathrm{dB}$ from rigid results. Modelling the blocked ear canal PRTFs with a monopole in the open ear canal leads to a better match with the measurement than the closed ear canal case. Repositioning the binaural microphones relates to MSD values of $2.03\,\mathrm{dB}$ between the measured PRTFs, which is lower than the MSD of measured and simulated data.

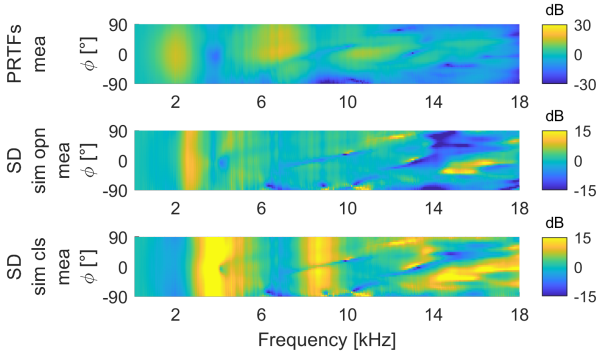

Figure 6: Measured (mea) frontal plane blocked PRTFs of the left ear and SD between mea and simulated (sim) PRTFs. In the simulations impedance BCs are used from the linearly fitted silicone and white resin samples $|R|$; the source is placed at the entrance of the open (opn) and closed (cls) ear canal.

Table 3: MSD of the measured and simulated PRTFs averaged over left and right ear in white and black resin. In the simulations rigid (rgd) and impedance (imp) BCs are used from the linearly fitted silicone, white and black resin samples $|R|$; the source is placed at the eardrum position and at the entrance of the open and closed ear canal (ec).

MSD [dB]	eardrum	open ec	closed ec
rigid	8.04	7.18	9.55
impedance	5.53	5.52	8.35

To assess if PRTFs from impedance BCs simulations relate to perceptual differences when compared to rigid results, the sagittal plane localisation model is employed. Defining the DTFs computed at the eardrum with rigid or impedance BCs as the template, i.e. the individual filters of the virtual subject, the QE and PE with all other PRTFs as targets are evaluated. The outcome, averaged over left and right ear in white and black material, is presented in Fig. 7 and compared to QE and PE ranges of minimal deviant nonindividual HRTFs. The blocked ear canal PRTFs show an overall increase in QE and PE from the eardrum data of at least $1.6\,\%$ and $0.7°$, respectively. Changes in BCs seem to have an influence on the localisation error,

although median error values always lie within the highlighted ranges. Using the rigid eardrum PRTFs as the template, as seen in Fig. 7a, matching PRTFs considering impedance BCs relate to mean increases in QE and PE of $6.2\,\%$ and $3.4°$, respectively. Smaller increases in QE and PE are observed when the PRTFs including impedance BCs are used as the template, as seen in Fig. 7b, with average values of $1.1\,\%$ and $0.2°$, respectively.

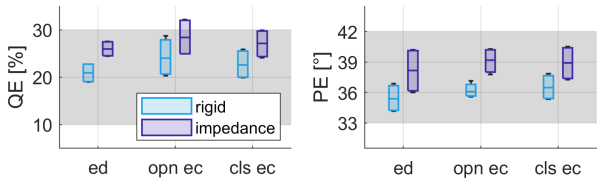

(a) Template: eardrum (ed) rigid PRTFs.

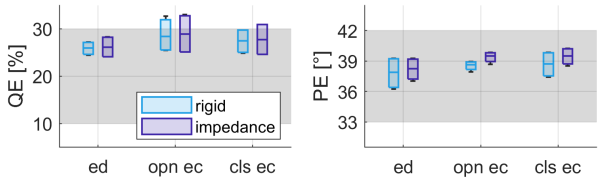

(b) Template: eardrum (ed) impedance PRTFs.

Figure 7: QE and PE of the simulated PRTFs averaged over left and right ear in white and black resin. In the simulations rigid and impedance BCs are used from the linearly fitted silicone, white and black resin samples $|R|$; the source is placed at the eardrum position (ed) and at the entrance of the open (opn) and closed (cls) ear canal (ec). The grey areas show QE and PE of minimal deviant nonindividual HRTFs.

4. DISCUSSION

The outcome of the analyses shows that simulations including impedance BCs up to $18\,\mathrm{kHz}$ relate to a better match to measured data than rigid simulations. Therefore, although several approximations are applied to correct artefacts in the impedance tube measurements, i.e. neglecting the phase and linearly fitting the results, the acquired $|R|$ seems to be valid in the tested frequency range. These artefacts can stem from challenges in measuring high acoustic impedance, requiring ideal measurement conditions [12]. An alternative calibration procedure of the impedance tube could potentially lead to a better estimation of the complex Z_s and further reduce the deviation between measured and simulated data [12]. Furthermore, impedance tubes are capable of measuring R only for normal incidence, deviating from the real scenario in which sound waves reach the outer ear from different directions. Inverse impedance identification techniques could be a promising alternative; however, modelling errors other than impedance mismatch might hinder their outcome [5]. Application of this approach to a simpler scenario, e.g. closed ear canal transfer functions, could lead to a more reliable impedance estimation.

The perceptual analysis results indicate that, when localising sound filtered with PRTFs deriving from impedance BCs simulations while having rigid PRTFs as templates, the localisation error is high. This error lies within ranges of minimal deviant nonindividual HRTFs, relating to small but significant perceptual differences [1]. The opposite case, akin to common virtual acoustic scene renderings in which a real subject is asked to localise sound filtered with numerical HRTFs, usually computed with rigid BCs, shows a minimal effect on QE and PE which would likely not alter the spatial sound perception. This behaviour could stem from the lack of damping in rigid PRTFs, relating to additional high frequency spectral features which could be used by the virtual subject to better localise a sound source. When the PRTFs with impedance BCs are used as the template these features are not known to the virtual subject; therefore, they cannot be used to improve localisation. Thus, rigid BCs simulations on accurate outer ear geometries are thought to lead to HRTFs that can be used for the creation of perceptually valid individual spatial audio. However, when using rigid simulations results as individual HRTFs in virtual experiments, the estimated localisation accuracy might be higher than with data originating from measurements or computations including realistic impedance BCs. Nonetheless, it should be stressed that the current results are obtained on outer ear replicas PRTFs of one subject, and additional analyses are needed on HRTFs computed on different geometries to validate and generalise the results. Furthermore, the use of replicas, although relating to more reproducible results, entails approximations potentially creating deviation from real subject measurements, e.g. different impedance values than human skin, which influence on spatial sound perception needs to be further assessed.

5. CONCLUSION

The acoustic impedance of material samples used to 3D print individual outer ear replicas was measured in an

impedance tube up to 20 kHz, showing a rigid behaviour similar to human skin. These impedance values were included as BCs in closed ear canal and PRTFs simulations up to 18 kHz, and their outcome shows a lower spectral difference from measured data than rigid computations. A perceptually inspired analysis between PRTFs obtained with rigid and impedance BCs shows that, when considering the latter as the reference, a minimal difference is obtained. The opposite case shows a higher discrepancy, probably relating to significant perceptual differences. Additional analyses considering HRTFs of different subjects are needed for generalisation purposes.

6. ACKNOWLEDGMENTS

The European Commission is gratefully acknowledged for their support of the VRACE research project (GA 812719). The research of S. van Ophem (fellowship no. 1277021N) is funded by a grant from the Research Foundation - Flanders (FWO). We would like to thank the researchers at Institut für Kommunikationstechnik, Leibniz Universität Hannover, for the help in the measurements.

7. REFERENCES

[1] C. Jenny and C. Reuter, "Usability of Individualized Head-Related Transfer Functions in Virtual Reality: Empirical Study With Perceptual Attributes in Sagittal Plane Sound Localization," *JMIR Serious Games*, vol. 8, no. 3, pp. 1–15, 2020.

[2] K. Pollack, W. Kreuzer, and P. Majdak, "Perspective Chapter: Modern Acquisition of Personalised Head-Related Transfer Functions - An Overview," in *Advances in Fundamental and Applied Research on Spatial Audio*, IntechOpen, 2022.

[3] B. F. G. Katz, "Acoustic absorption measurement of human hair and skin within the audible frequency range," *The Journal of the Acoustical Society of America*, vol. 108, no. 5, pp. 2238–2242, 2000.

[4] A. B. Dobrucki and P. Plaskota, "Computational Modelling of Head-Related Transfer Function," *Archives of Acoustics*, vol. 32, no. 3, pp. 659–682, 2007.

[5] S. Ghorbal, X. Bonjour, and R. Séguier, "On the importance of impedance for perceptual relevance of HRTF," in *Proc. of 148th AES Convention*, 2020.

[6] R. Schlieper, T. Gnadeberg, S. Li, S. Preihs, and J. Peissig, "High-frequency acoustic impedance tube based on MEMS microphones," in *Proc. of INTER-NOISE 2021*, pp. 4724–4732, 2021.

[7] R. Roden and M. Blau, "The IHA database of human geometries including torso, head and complete outer ears for acoustic research," in *Proc. of INTER-NOISE 2020*, pp. 4226–4237, 2020.

[8] D. Sinev, F. Di Giusto, J. Peissig, S. van Ophem, and E. Deckers, "Individual Ear Replicas with Complete Ear Canals Compatible with an Artificial Head," in *Proc. of DAGA 2023*, pp. 166–169, 2023.

[9] H. Takemoto, P. Mokhtari, H. Kato, R. Nishimura, and K. Iida, "Mechanism for generating peaks and notches of head-related transfer functions in the median plane," *The Journal of the Acoustical Society of America*, vol. 132, no. 6, pp. 3832–3841, 2012.

[10] K. Pollack, F. Di Giusto, D. Sinev, and P. Majdak, "Spectral and psychoacoustic evaluation of head-related transfer functions calculated at the blocked ear canal and the eardrum," in *Proc. of Forum Acusticum 2023 (submitted)*, 2023.

[11] D. Sinev, F. Di Giusto, K. Pollack, K. Mick, and J. Peissig, "Assessment of the Directional Characteristics of the Ear Canal Using 3D Printed Replicas and Numerical Simulations," in *Proc. of Forum Acusticum 2023 (submitted)*, 2023.

[12] R. Schlieper, L. Misterek, S. Preihs, and J. Peissig, "Analysis of resonance free calibration methods for acoustic impedance measurements with respect to signal-to-noise ratio and temperature drift," *Manuscript submitted for publication*, 2023.

[13] L. L. Beranek and T. J. Mellow, *Acoustics: Sound Fields and Transducers*. Academic Press, 2012.

[14] COMSOL AB, "Acoustics Module User's Guide," 2021.

[15] G. A. Haidar, X. Moreau, and R. A. Z. Daou, "Analysis of the Effects of the Viscous Thermal Losses in the Flute Musical Instruments," *Fractal and Fractional*, vol. 5, no. 1, pp. 1–20, 2021.

[16] R. Baumgartner, P. Majdak, and B. Laback, "Modeling sound-source localization in sagittal planes for human listeners," *The Journal of the Acoustical Society of America*, vol. 136, pp. 791–802, 2014.